https://doi.org/10.30799/jnst.130.18040409 J. Nanosci. Tech. - Volume 4 Issue 4 (2018) 435–438

ISSN: 2455-0191

Share Your Innovations through JACS Directory

Journal of Nanoscience and Technology

Visit Journal at http://www.jacsdirectory.com/jnst

Synthesis and Characterization of Nano Ag_2O and $Cu(OH)_2$ by Solution Reduction Method and Their Antibacterial Studies

R. Rajakumari*, C. Priya, A. Srilekha

PG and Research Department of Physics, Queen Mary's College (Autonomous), Chennai – 600 004, Tamil Nadu, India.

ARTICLE DETAILS

Article history:
Received 23 June 2018
Accepted 04 July 2018
Available online 22 July 2018

Keywords:
Solution Reduction Method
Ferromagnetic Interaction
Antibacterial Studies

ABSTRACT

Silver oxide (Ag_2O) and copper(II)hydroxide ($Cu(OH)_2$) nanoparticles were synthesized through a simple solution reduction method using silver nitrate ($AgNO_3$) and copper sulphate pentahydrate ($CuSO_4.5H_2O$) in the presence of sodium hydroxide (NaOH) as reducing agent. X-ray diffraction (XRD) analysis, scanning electron microscopic (SEM) analysis, Fourier transform infrared spectroscopic (FT-IR) analysis, UV-absorption and photoluminescence (PL), vibrating sample magnetometer (VSM) studies were performed to confirm the size distribution measurement, surface morphology, optical and magnetic properties of the synthesized samples. Silver nanoparticles synthesized in the form of Ag_2O and copper in the form of $Cu(OH)_2$ was confirmed by the XRD study. The UV-Vis absorption analysis indicates that the absorption peak for Ag_2O in the lower wavelength region of the optical spectrum. The sharp intensity peaks in the FTIR spectrum of Ag_2O and $Cu(OH)_2$ indicate the stretching and bending frequencies of the molecular functional groups in the samples as well as their high crystalline nature. The SEM images show the shape of Ag_2O nanoparticles is nearly spheroid. The VSM study of $Cu(OH)_2$ shows ferromagnetic interaction at room temperature. The antibacterial properties of Ag_2O and $Cu(OH)_2$ on *Staphylococcus aureus* and *Escherichia coli* indicate that both the samples are effective on *Staphylococcus aureus*, which is concentration dependent.

1. Introduction

The noble metal nanoparticles have been the subject of focused research due to their unique optical, electronic, mechanical, magnetic, and chemical properties that are significantly different from those of bulk materials [1]. Preparation of silver nanoparticles has attracted particularly considerable attention due to their diverse properties and uses, like magnetic and optical polarizability [2], electrical conductivity [3], catalysis [2], antimicrobial and antibacterial activities [4-5], DNA sequencing [6], and surface-enhanced Raman scattering (SERS) [7].

Nano scale copper compounds are of research interest for the many applications. Synthesis of copper compounds at nano scale has been actively researched for many decades, this is because, it is an important industrial material and it has novel physical and chemical properties. Among all metals used in modern electronic circuits, Cu is the most common one because of its excellent electrical conductivity and low cost. Copper compounds are one of the most normal conductors in modern technologies and could be used widely in nano device. Therefore, the development of uniform copper compound nanoparticles has been intensively pursued [8]. Copper hydroxide [$Cu(OH)_2$] nanoparticle is one of the copper compounds and it has many applications. One of the main uses for $Cu(OH)_2$ is a fungicide and nematicide. $Cu(OH)_2$ is the most toxic compound against *E. vermiculata* [9]. People also use it for insecticides for walnuts, wine grapes, and peaches among many other types of fruits and nuts commonly grown for agricultural purposes throughout the world. $Cu(OH)_2$ is used as fungicide on fruits, vegetables, ornamentals, the manufacture of rayon, as a source for copper salts, as a mordant, kill mold in paints. It can be used to color ceramics, as a catalyst, as an alternative to the bordeaux mixture, nematicide. $Cu(OH)_2$ is also occasionally used as ceramic colorant, combined with latex paint, making a product designed to control root growth in potted plants [8,9]. Synthesis of $Cu(OH)_2$ nanoparticles attracted increased attention due to reliable low cost, specific size, well-defined morphologies and wide range of potential applications. Various methods of synthesis of $Cu(OH)_2$ nanoparticles include, biosynthesis [10], chemical co-precipitation method [11], a two-step template approach [12], wet chemical route [13, 14], anion exchange method [15], and an electrochemical method [16, 17] have been reported.

The most common and simplest bulk-solution synthetic method that has been used for the preparation of metal nanoparticles is chemical reduction of metal salts. For the synthesis of nanoparticles, soluble metal salt is generally used as a reducing agent, and a stabilizing agent (caps the particle and prevents further growth of the particle or aggregation). It was, therefore, thought worthwhile to prepare Ag_2O and $Cu(OH)_2$ nanoparticles for its various applications through simple chemical modification using Sodium hydroxide (NaOH), Silver nitrate ($AgNO_3$) and Copper sulphate pentahydrate ($CuSO_4.5H_2O$). In the present study NaOH was used as the reducing agent.

2. Experimental Methods

The Ag_2O and $Cu(OH)_2$ nanoparticles were produced using starting materials such as $AgNO_3$, $CuSO_4.5H_2O$ and NaOH pellets (Merck, Mumbai, India). All the chemicals were of analytical grades and used without further purification.

2.1 Synthesis of Ag_2O and $Cu(OH)_2$ Nanoparticles

To synthesize Ag_2O nanoparticles, 2.195 g of $AgNO_3$ and 0.4 g of NaOH were dissolved in 20 mL of distilled water separately at the ratio of 5:1. The NaOH solution was taken in a burette and the $AgNO_3$ solution was taken in a beaker. The solution was allowed to be stirred (990 rpm) for 2 hours at room temperature and NaOH was added drop-wise into to the solution simultaneously. Immediate color change was observed when NaOH was added into $AgNO_3$. This mixture was sonicated for 30 min and centrifuged for five times with distilled water and ethanol at the rpm rate of 800. The resultant precipitate was filtered and dried in an oven for an hour at 100 °C to get Ag_2O nanoparticles. In summary, the following chain reaction accompanies the whole process $AgO \rightarrow Ag_2O \leftrightarrow Ag + O$, $AgO + Ag \rightarrow Ag_2O$. The same protocol was followed for the synthesis of $Cu(OH)_2$. Instead of $AgNO_3$, $CuSO_4.5H_2O$ was used as the starting material. In both the cases, NaOH was used as the reducing agent.

*Corresponding Author:raj_mtwu30@yahoo.co.in(R. Rajakumari)

https://doi.org/10.30799/jnst.130.18040409
2455-0191 / JACS Directory©2018. All Rights Reserved

Cite this Article as: R. Rajakumari, C. Priya, A. Srilekha, Synthesis and characterization of nano Ag_2O and $Cu(OH)_2$ by solution reduction method and their antibacterial studies, J. Nanosci. Tech. 4(4) (2018) 435–438.

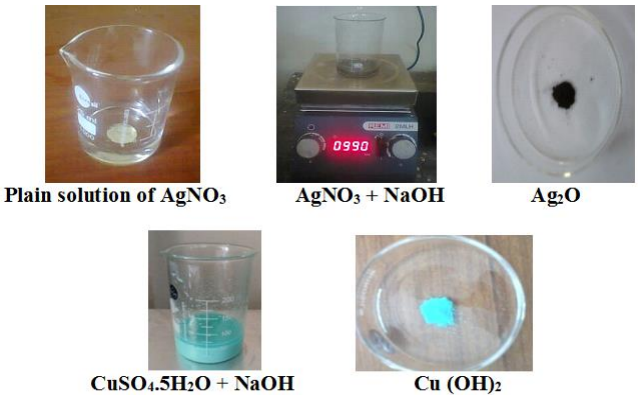

Fig. 1 Photos of Ag_2O and $Cu(OH)_2$ Nanopowder

3. Results and Discussion

3.1 Structural Analysis

The structural analysis of the samples was studied using XRD analysis. Fig. 2 shows the XRD pattern recorded from powder samples of Ag_2O and $Cu(OH)_2$. XRD pattern of Ag_2O reveals that the sample is nano sized and crystalline. The fine particle nature of the sample is reflected in the X-ray line broadening. The experimental diffraction angle (2θ) of the specimen is consistent with the standard diffraction angle (2θ) of the specimen. Five peaks at 2θ values of 32.9885°, 38.2556°, 55.1869°, 66.0084°, 69.2414° corresponding to (111), (200), (220), (311), and (222) planes of Ag_2O are observed. The observed XRD data is compared with the standard powder diffraction card JCPDS file No. 41-1104. The three strongest lines ((111), (200) and (220)) with the d- spacing (2.715 Å, 2.352 Å and 1.66 Å) in the XRD pattern is in good agreement with standard values (2.73 Å, 2.36 Å and 1.67 Å) of Ag_2O.The experimental diffraction angle (2θ) of $Cu(OH)_2$ is in good agreement with the standard diffraction angle (2θ) of the specimen. Five peaks at 2θ values of 16.6438°, 22.8704°, 28.0885°, 34.5357°, 35.6738° corresponding to (020), (021), (110), (002), and (111) planes of $Cu(OH)_2$ are observed. The observed XRD data is compared with the standard powder diffraction card JCPDS, Cu $(OH)_2$ file No. 35-0505. The crystallite size of Ag_2O and $Cu(OH)_2$ was calculated using Scherer equation. The average crystallite size of both the samples was found to be 26 nm and 21 nm respectively.

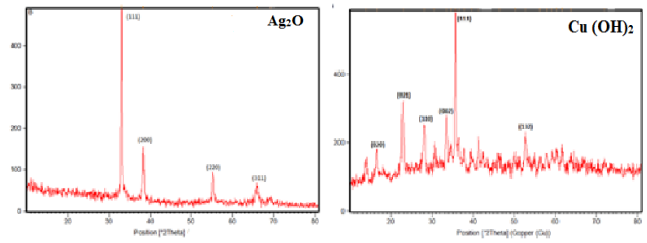

Fig. 2 XRD pattern of Ag_2O and $Cu(OH)_2$

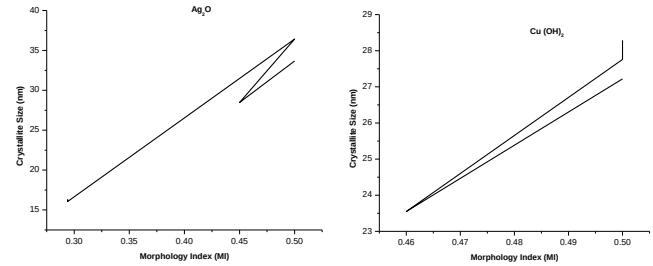

Fig. 3 Morphology index (vs) crystallite size for Ag_2O and $Cu(OH)_2$

3.2 XRD- Morphology Index, Lorentz Factor, Lorentz Polarization Factor

A XRD morphology index (MI) is developed from FWHM of XRD data of the synthesized samples. MI relates the FWHM of two peaks to its particle morphology (peak having highest FWHM and a particular peak's FWHM for which MI is calculated). Generally, highest FWHM peak MI is 0.5 because the MI is derived from the single peak only. MI is obtained using Eq.(1). The value of MI ranges from 0.2 to 0.5 for experimental Ag_2O nanopowder, and the details are presented in Table1. It is correlated with the crystallite size. The result shows that morphology index has direct relationship with crystallite size. For $Cu(OH)_2$, the value of MI is 0.5 and it is presented in Table 2. These results are shown in Fig. 3.

$$MI = \frac{FWHM_h}{FWHM_h + FWHM_p} \quad (1)$$

Lorentz factor (LF) is a multiplicative factor involved in converting diffracted radiation intensities in to structure factors during the process of structure determination in XRD experiments, involving moving crystals. Controlling X-ray intensities of diffraction angles needs to be monitored, hence Lorentz-polarization factor (LPF) was introduced. In the intensity calculations, Lorentz factor is combined with the polarization factor and further the variation of the LF with the Bragg angle (θ) is shown [18, 19]. The overall effect of LF is to decrease the intensity of the reflections at intermediate angles compared to those in the forward or backward directions. LF and LPF are calculated from Eqs.(2) and (3) and tabulated in Tables 1 and 2 for Ag_2O and $Cu(OH)_2$ nanoparticles. It is observed that, the values of LF and LPF decrease as the angle of diffraction increases.

$$Lorentz\ Factor = \frac{\cos\theta}{\sin^2(2\theta)} \quad (2)$$

$$Lorentz\ Polarization\ Factor = \frac{1+\cos^2(2\theta)}{\sin^2(\theta)\cos(\theta)} \quad (3)$$

3.3 XRD - Dislocation Density

The dislocation density is defined as the length of dislocation lines per unit volume of the crystal. In materials science, a dislocation is a crystallographic defect, or irregularity, within a crystal structure. The presence of dislocations strongly influences many of the properties of materials. The movement of a dislocation is impeded by other dislocations present in the sample. Thus, a larger dislocation density implies a larger hardness. The X-ray line profile analysis has been used to determine the dislocation density. The dislocation density can also be calculated from equations (4)

$$\delta = \frac{1}{D^2} \quad (4)$$

where, δ is dislocation density and D is the crystallite size. In the present study, the dislocation density is of the order of 10^{14} m^{-2} (Table 1). It is known that annealed crystals have a dislocation density of about 10^8 m^{-2}. This can be increased to 10^{10} - 10^{12} m^{-2} by moderate cold working and to 10^{14} - 10^{16} m^{-2} by heavy cold working. As the dislocation density increases, the stress required to move any one dislocation increases due to the interfering effect of the stress fields of the surrounding dislocations. This phenomenon is the basis of work hardening.

Table 1 Crystallite size, MI, LF and LPF values of Ag_2O

2θ (degree)	h k l	Crystallite size (nm)	Morphology Index	Lorentz Factor	Lorentz Polarization Factor	Dislocation Density $\delta = 1/D^2$ ($10^{14}m^{-2}$)
32.9885	(111)	33.67	0.500	3.2344	22.039	8.820
38.2556	(200)	28.48	0.450	2.4644	15.936	12.23
55.1869	(220)	36.43	0.500	1.3148	6.9734	7.530
66.0084	(311)	16.06	0.294	1.0047	4.6834	38.77
69.2444	(222)	16.36	0.294	0.9410	4.2367	37.36

Table 2 Crystallite size, MI, LF and LPF values of $Cu(OH)_2$

2θ (degree)	h k l	Crystallite size (nm)	Morphology Index	Lorentz Factor	Lorentz Polarization Factor	Dislocation Density $\delta = 1/D^2$ ($10^{15}m^{-2}$)
16.6438	(020)	27.22	0.50	12.06	92.53	1.349
22.8704	(021)	23.55	0.46	6.489	48.12	1.803
28.0885	(110)	27.76	0.50	4.376	31.13	1.298
33.4381	(002)	28.12	0.50	3.154	21.40	1.265
35.6738	(111)	28.29	0.50	2.799	18.58	1.249

3.4 UV- Vis Absorption Analysis of Ag_2O and $Cu(OH)_2$

The UV -vis absorption spectra of Ag_2O and $Cu(OH)_2$ is shown in Fig. 4. It is observed that no prominent peaks are seen in the visible range of the UV -vis absorption spectra of both Ag_2O and $Cu(OH)_2$. It is also observed that λ_{max} is only in the UV range for both the samples and this may be due to the agglomeration of particles, and the oxidized form of the samples. The cut off wavelengths (where the absorption value is small) are 305 nm and 400 nm respectively for Ag_2O and $Cu(OH)_2$.

https://doi.org/10.30799/jnst.130.18040409

Cite this Article as: R. Rajakumari, C. Priya, A. Srilekha, Synthesis and characterization of nano Ag_2O and $Cu(OH)_2$ by solution reduction method and their antibacterial studies, J. Nanosci. Tech. 4(4) (2018) 435–438.

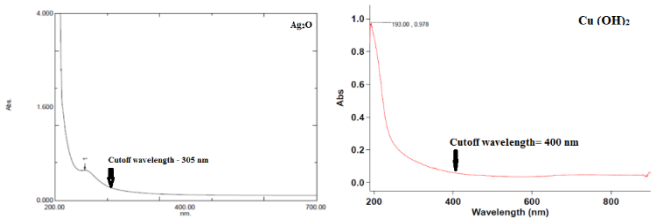

Fig. 4 UV-Vis absorption spectra of Ag_2O and $Cu(OH)_2$

3.5 FTIR Analysis of Ag_2O and $Cu(OH)_2$

The FTIR spectrum of Ag_2O is shown in Fig. 5. The absorption bands in the region of 500 to 600 cm^{-1} include those for crystal (lattice) and coordinated water as well as Ag_2O. The absorption bands for Ag_2O are weak and overlap with those of rotational H-O-H vibration and vibrational of trapped H_2O. The asymmetric and symmetric stretching H-O-H vibration bands are observed at 3,100 cm^{-1}. The doublet band at approximately 1,400 cm^{-1} can be ascribed to H-O-H bending vibrations. The bands, observed between 855 and 702 cm^{-1}, can be attributed to the bending vibrational modes (wagging, twisting, and rocking) of coordinated water molecules.

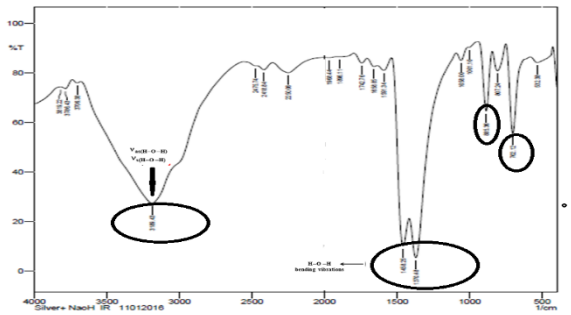

Fig. 5 FTIR spectrum of Ag_2O

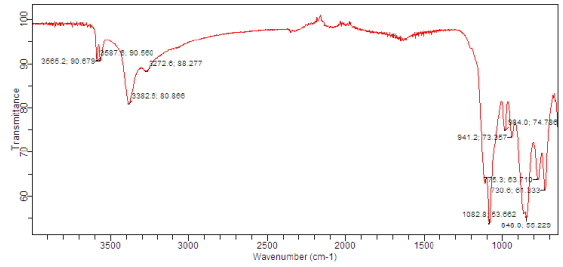

Fig. 6 FTIR spectrum of $Cu(OH)_2$

The FTIR spectrum for $Cu(OH)_2$ (Fig. 6) shows a peak at 3565.90 cm^{-1} corresponding to the free O-H group. Another strong and sharp peak with a maximum of 3382.90 cm^{-1} is due to the hydrogen bonded hydroxyl groups and bending mode of the hydroxyl group of water. The spectrum also shows a strong peak at 1082.53 cm^{-1} indicating strong SO_4 stretching and the peak at 845.55 cm^{-1} indicates Cu-OH vibrations.

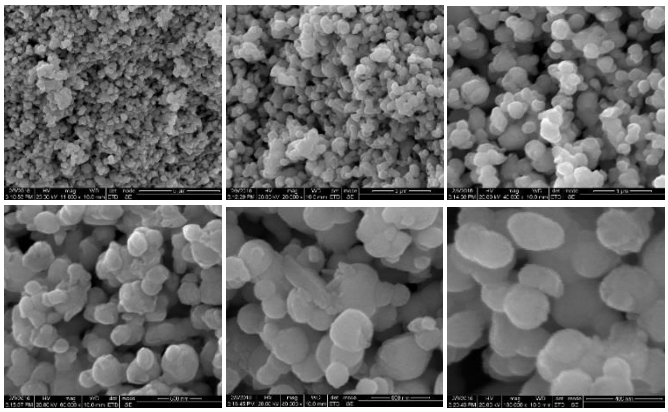

Fig. 7 SEM Images of Ag_2O Nanopowder

3.6 SEM Analysis of Ag_2O

SEM images (Fig. 7) of Ag_2O nanopowder, obtained from chemical reduction method obviously show that the tendency of nanoparticles to agglomerate decreases. The shape of the nanoparticle is spheroid. The size of the nanoparticles obtained from the given scaling is 40 nm.

3.7 VSM Study of $Cu(OH)_2$

The VSM study of $Cu(OH)_2$ shows ferromagnetic interaction at room temperature (Fig. 8). This is a relaxed ferromagnetic effect due to decrease in the size of the particle as well as due to magnetostriction effect. It is also observed that the area of the hysteresis loop is narrow, which indicates the soft magnetic behavior of the sample. The value of coercivity is 482.35 Gauss and the value of retentivity is 191.10×10^{-6} emu.

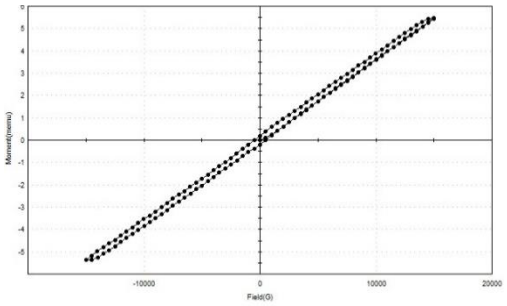

Fig. 8 M-H curve of $Cu(OH)_2$

3.8 Antibacterial Activity of Ag_2O and $Cu(OH)_2$ Nanoparticles

The antibacterial effects of Ag_2O and $Cu(OH)_2$ nanoparticles have been tested with two bacterial strains *Staphylococcus aureus* and *Escherichia coli* at various concentrations (500,100,50,10,5, and 1 µg/mL). Of the two synthesized samples, Ag_2O was effective against *Staphylococcus aureus* in comparison with $Cu(OH)_2$ (Fig. 9). From the present study, it is also observed that the effect is concentration dependent (Table 3). On the other hand, both the samples had no effect on *Escherichia coli* (Table 4). Ag_2O had inhibition zone of 17 mm at higher concentration of 500 µg/mL on the bacterial strain *Escherichia coli.*

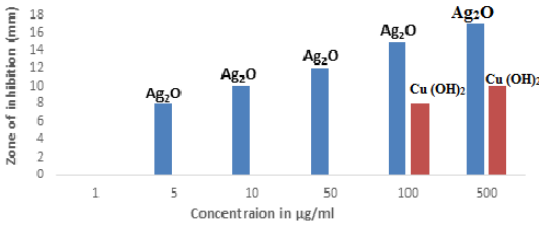

Fig. 9 Concentrations of Ag_2O & $Cu(OH)_2$ nanoparticles in µg/mL (vs) zone of inhibition in mm

Table 3 Antibacterial activity of the Ag_2O and $Cu(OH)_2$ against *Staphylococcus aureus* ATCC 25923 standard strains

Compound	Concentration (µg/mL)					
	500	100	50	10	5	1
Ag_2O	17 mm	15 mm	12 mm	10 mm	8 mm	No Zone
$Cu(OH)_2$	10 mm	8 mm	No Zone	No Zone	No Zone	No Zone

Table 4 Antibacterial activity of the compounds against *Escherichia coli* ATCC 25922 standard strains

Compound	Concentration (µg/mL)					
	500	100	50	10	5	1
Ag_2O	16 mm	No Zone	No Zone	No Zone	No Zone	No Zone
$Cu(OH)_2$	No Zone	No Zone	No Zone	No Zone	No Zone	No Zone

4. Conclusion

Ag_2O and $Cu(OH)_2$ nanoparticles were successfully syntheisized by simple solution reduction method. The powder XRD patterns of both the samples indicate the well cystalline nature of the samples and also in good agreement with their characteristic peaks. The crystallite size calculated using Scherer equation was 21 nm and 27 nm, respectively, for Ag_2O and $Cu(OH)_2$. The absorption peaks in the UV range of both the samples, observed from UV absorpton analysis indicate the agglomeration of the particles and oxidized form of the samples as well. The SEM images of Ag_2O show nealy spherical nanoparticles of size 40 nm. The VSM study of $Cu(OH)_2$ showed relaxed ferromagnetic interaction at room temperature, inspite of Cu being a paramagnetic material. The Ag_2O and $Cu(OH)_2$ nanoparticles were tested for their antibacterial activity on the bacterial strains *Staphylococcus aureus* and *Escherichia coli* upon varying their

https://doi.org/10.30799/jnst.130.18040409

Cite this Article as: R. Rajakumari, C. Priya, A. Srilekha, Synthesis and characterization of nano Ag_2O and $Cu(OH)_2$ by solution reduction method and their antibacterial studies, J. Nanosci. Tech. 4(4) (2018) 435–438.

concentrations. The Ag_2O nanoparticles showed zone of inhibition on *Staphylococcus aureus*, which was concentration dependent. $Cu(OH)_2$ nanoparticles had zone of inhibition only on the higher concentrations of 100 µg/mL and 500 µg/mL. Both the samples had no effect on *Escherichia coli* even at higher concentrations.

Acknowledgement

The author (RR) wish to acknowledge University Grants Commission (New Delhi, India) for providing financial support in the form of Minor Research Project.

References

[1] M. Mazur, Electrochemically prepared silver nanoflakes and nanowires, Electrochem. Comm. 6 (2004) 400-403.
[2] Y. Shirish, N. Toshima, Oxidation of ethylene catalyzed by colloidal dispersions of poly(sodium acrylate)-prepared silver nanoclusters, Colloid Surf. A: Physicochem. Eng. Aspect. 169 (2000) 59-66.
[3] L.T. Chang, C.C. Yen, Studies on the preparation and properties of conductive polymers, Use of heat treatment to prepare metalized films from silver chelate of PVA and PAN, J. Appl Polym. Sci. 55 (1995) 371-374.
[4] C. Baker, A. Pradhan, L. Pakstis, D.J. Pochan, S.I. Shah, Synthesis and antibacterial properties of silver nanoparticles, J. Nanosci. Nanotechnol. 5 (2005) 224-249.
[5] A.R. Shahverdi, S. Mianaeian, H.R. Shahverdi, H. Jamalifar, A.A. Nohi, Rapid synthesis of silver nanoparticles using culture supernatants of enterobacteria: A novel biological approach, Proc. Biochem. 42 (2007) 919-923.
[6] Y.W. Cao, R. Jin, C.A. Mirkin, DNA-modified core-shell Ag/Au nanoparticles, J. Am. Chem. Soc. 123 (2001) 7961-7962.
[7] P. Matejka, B. Vlckova, J. Vohlidal, P. Pancoska, V. Baumuruk , The role of Triton X-100 as an adsorbate and a molecular spacer on the surface of silver colloid: a surface-enhanced Raman scattering study, J. Phys. Chem. 96 (1992) 1361-1366.
[8] R.H.P. Devamani, M. Alagar, Synthesis and characterization of copper II hydroxide nanoparticles, Nano Biomed. Eng. 5 (2013) 116-120.
[9] E.H. Eshra, Toxicity of methomyl, copper hydroxide and urea fertilizer on some land snails, Ann. Agric. Sci. 59 (2014) 281-284.
[10] A.M. Awwad, A. Borhan, Biosynthesis of colloidal copper hydroxide nanowires using Pistachio leaf extract, Adv. Mater. Lett. 6 (2015) 51-54.
[11] G.H. Du, G.V. Tendeloo, $Cu(OH)_2$ nanowires, CuO nanowires and CuO nanobelts, Chem. Phys. Lett. 393 (2004) 64-69.
[12] C. Lu, L. Qi, J. Yang, D. Zhang, N. Wu, J. Ma, Simple template-free solution route for the controlled synthesis of $Cu(OH)_2$ and CuO nanostructures, J. Phys. Chem. B. 108 (2004) 17825-17831.
[13] D.P. Singh, A.K. Ojha, O.N. Srivastava, Efficient catalytic effect of CuO nanostructures on the degradation of organic dyes, J. Phys. Chem. C 113 (2009) 3409-3418.
[14] W. Wang, C. Lan, Y. Li, K. Hong, G. Wang, A simple wet chemical route for large-scale synthesis of $Cu(OH)_2$ nanowires, Chem. Phys. Lett. 366 (2002) 220-223.
[15] S.H. Park, H.J. Kim, Unidirectionally aligned copper hydroxide crystalline nanorods from two-dimensional copper hydroxy nitrate, J. Am. Chem. Soc. 126 (2004) 14368-14369.
[16] D.D. La, S.Y. Park, Y.W. Choi, Y.S. Kim, Wire-like bundle arrays of copper hydroxide prepared by the electrochemical anodization of Cu foil, Bull. Korean Chem. Soc. 31 (2010) 2283-2288.
[17] V.K. Vidhu, S.A. Aromal, D. Philio, Green synthesis of silver nanoparticles using *Macrotyloma uniflorum*, Spectrochim. Acta A 83 (2011) 392-397.
[18] H. Peiser. H.P. Rooksby, A.J.C. Wilson, X-Ray diffraction by polycrystalline materials, the institute of physics, IOP Pub, London, 1955.
[19] G.L .Clark, Applied X-rays, 4th Edn., McGraw- Hill Book Company, Inc., New York, 1955.

https://doi.org/10.30799/jnst.130.18040409

Cite this Article as: R. Rajakumari, C. Priya, A. Srilekha, Synthesis and characterization of nano Ag_2O and $Cu(OH)_2$ by solution reduction method and their antibacterial studies, J. Nanosci. Tech. 4(4) (2018) 435–438.